IVYSPRING INTERNATIONAL PUBLISHER

Theranostics

2020; 10(6): 2631-2644. doi: 10.7150/thno.40808

Review

Near-IR emissive rare-earth nanoparticles for guided surgery

Zhibei Qu[1,2], Jianlei Shen[2], Qian Li[2], Feng Xu[1], Fei Wang[1,2], Xueli Zhang[1]✉, Chunhai Fan[2]✉

1. Joint Research Center for Precision Medicine, Shanghai Jiao Tong University & Affiliated Sixth People's Hospital South Campus, Southern Medical University Affiliated Fengxian Hospital, Shanghai 201499, China.
2. School of Chemistry and Chemical Engineering, and Institute of Molecular Medicine, Renji Hospital, School of Medicine, Shanghai Jiao Tong University, Shanghai 200240, China.

✉ Corresponding authors: fanchunhai@sjtu.edu.cn; lejing1996@aliyun.com

Received: 2019.10.01; Accepted: 2019.11.01; Published: 2020.02.03

Abstract

Intraoperative image-guided surgery (IGS) has attracted extensive research interests in determination of tumor margins from surrounding normal tissues. Introduction of near infrared (NIR) fluorophores into IGS could significantly improve the *in vivo* imaging quality thus benefit IGS. Among the reported NIR fluorophores, rare-earth nanoparticles exhibit unparalleled advantages in disease theranostics by taking advantages such as large Stokes shift, sharp emission spectra, and high chemical/photochemical stability. The recent advances in elements doping and morphologies controlling endow the rare-earth nanoparticles with intriguing optical properties, including emission span to NIR-II region and long life-time photoluminescence. Particularly, NIR emissive rare earth nanoparticles hold advantages in reduction of light scattering, photon absorption and autofluorescence, largely improve the performance of nanoparticles in biological and pre-clinical applications. In this review, we systematically compared the benefits of RE nanoparticles with other NIR probes, and summarized the recent advances of NIR emissive RE nanoparticles in bioimaging, photodynamic therapy, drug delivery and NIR fluorescent IGS. The future challenges and promises of NIR emissive RE nanoparticles for IGS were also discussed.

Key words: near infrared fluorescence; rare earth nanoparticle; bioimaging; image guided surgery

1. Introduction

Surgical operation is one of the most frequently used therapy to cancer treatment for centuries [1,2]. In common cancer surgeries, intraoperative evaluation of margins of tumor is essential to determine the final curative result [3]. However, it is mainly dependent on the visual senses and subjective palpation to decide excision [4] during the surgical operation. Inevitably, it is very difficult for the surgeons to discriminate the tumor margins from surrounding normal tissues [5,6]. It has been reported that tumor recurrence happens as high as 20-30% after surgical therapy, and subsequent cancer metastasis largely increases the complexity [7,8]. It is highly demanded to maximize tumor removal, minimize damage to the normal tissues and shorten surgical time [9]. Thus, intraoperative image-guided surgery (IGS) [5,10,11] is introduced to provide real-time tumor visualization to oncological surgeons to do them a favor in cancer margin recognition[12].

Among various optical imaging techniques [13], near-infrared (NIR) fluorescence imaging [14,15] is one of the latest trends in IGS applications[16], for use in both fundamental medical research and clinical practice[17,18]. Due to advantages in reduction of light scattering, photon absorption and autofluorescence *via* broadening to the 700–1,700 nm NIR window [19], NIR fluorescence-based imaging technique provides high spatial resolution along with increased tissue penetration depths. Very recently, NIR phosphors that extended to the entire NIR

window, including small molecules [20–22], inorganic nanoparticles [23,24], organic macromolecules [25,26] and quantum dots (QDs) [27,28] with tunable emission wavelength were developed [29]. Besides the benefits of efficient detection of NIR photons, recently developed NIR fluorophores have enabled biomedical imaging [30] of specific biomarkers [31] and anatomical structures with better signal-to-noise ratio, application for preclinical animal studies [32,33], clinical diagnostics [34] and translational medicine [35].

Compared with the visible spectrum widely employed for fluorescence imaging, the studies over the broadly defined NIR window are still in their infancy [36]. In the past decade, researches in NIR fluorescence imaging have focused on the conventional NIR window (NIR-I, 700-900 nm)[37], and have recently extended their efforts to the second NIR window (NIR-II, 1,000-1,700 nm)[38,39]. The NIR-I window is typically named as the 'biological transparent window' because in this range there is low tissue absorption and fluorescence background *in vivo* (compared with the visible range)[40]. The studies of molecular imaging to the novel NIR-II window has been achieved by the development of biocompatible NIR fluorophores with increasingly longer wavelengths throughout the field of chemistry, materials science and nanotechnology [41]. Also, we shall thank to the development of more efficient photon detectors with high NIR-II sensitivity as well as the drop of the price. It is more and more widely accepted that *in vivo* NIR-II fluorescence technology is superior to traditional NIR-I one due to the further reduced scattering, absorption and tissue autofluorescence [42].

Among the existed NIR materials, Rare earth (RE) nanoparticles [43,44] can afford good stability, ease to fabricate [45,46], high emissive efficiency [47] and long luminescence lifetime to microseconds[48]. Compared with lanthanide chelates [49], QDs [50,51], polymers [52], and organic dyes [53,54], lanthanide-doped inorganic RE nanoparticles hold all the advantages, including tunable emission[55], large Stokes shift [56], sharp emission peaks [57], and high chemical/photochemical stability [58] (Figure 1). Moreover, facile to multiple choices of doping [59], RE-doped inorganic materials can provide efficient emission from the ultraviolet (UV), passing through the whole visible range, to the mid-infrared region upon excitation [55,60,61]. All the advantages mentioned above have enabled the promising potential of NIR emissive RE nanoparticles in bioimaging [62], theranostics [63,64], photothermal therapy [65,66], drug delivery [67], and also the clinical IGS [20,68].

In this review, we provided a comprehensive introduction to the RE based NIR emissive nanoparticles. We systematically compared the benefits and of RE nanoparticles with other NIR probes, and summarized the recent advances of NIR emissive RE nanoparticles in bioimaging, photodynamic therapy, drug delivery and NIR fluorescence enabled IGS. The future challenges and promises of RE nanoparticles with NIR emission were also discussed.

2. NIR emissive rare earth nanoparticles

2.1. Emission mechanism of RE nanoparticle

RE nanoparticles are important fluorescent materials, due to their ability to enable intriguing emission properties, including tunable fluorescence color (Figure 1) [70,73], long life-time photoluminescence [74], highly efficient upconversity [75], long persistent phenomenon [76,77]. Generally speaking, RE elements are composed of 15 lanthanides (from lanthanum to lutetium), and usually plus scandium and yttrium. With abundant *f* shell orbitals, trivalent lanthanide (Ln) ions can exhibit sharp fluorescent emissions through intra-4*f* or 4*f*-5*d* transitions and thus are widely used as emitting centers in many fluorophores [78]. There are multiple methods to endow RE nanoparticles with NIR emission, using either upconversion [79] or down-shifting mechanisms (Figure 1) [69], and even long lifetime fluorophore and "after-glow" persistent luminescence [80–82]. Various luminescence features have been achieved in a wide spectrum of matrix materials, such as RE oxides, fluorides, and other matrices.

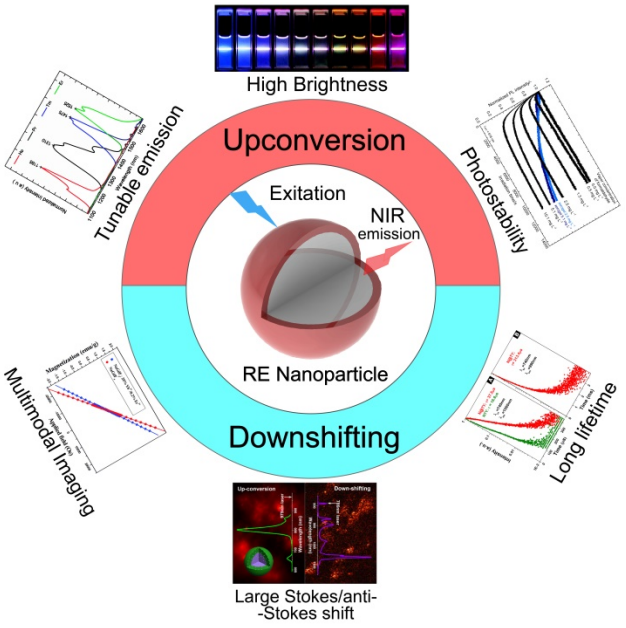

Figure 1. Characteristic properties of NIR emissive RE nanoparticles. Inset figures were adapted from Ref [63,69–72]. Copyright 2014, Royal Society of Chemistry; Copyright 2008, 2011, 2013, 2016, American Chemical Society.

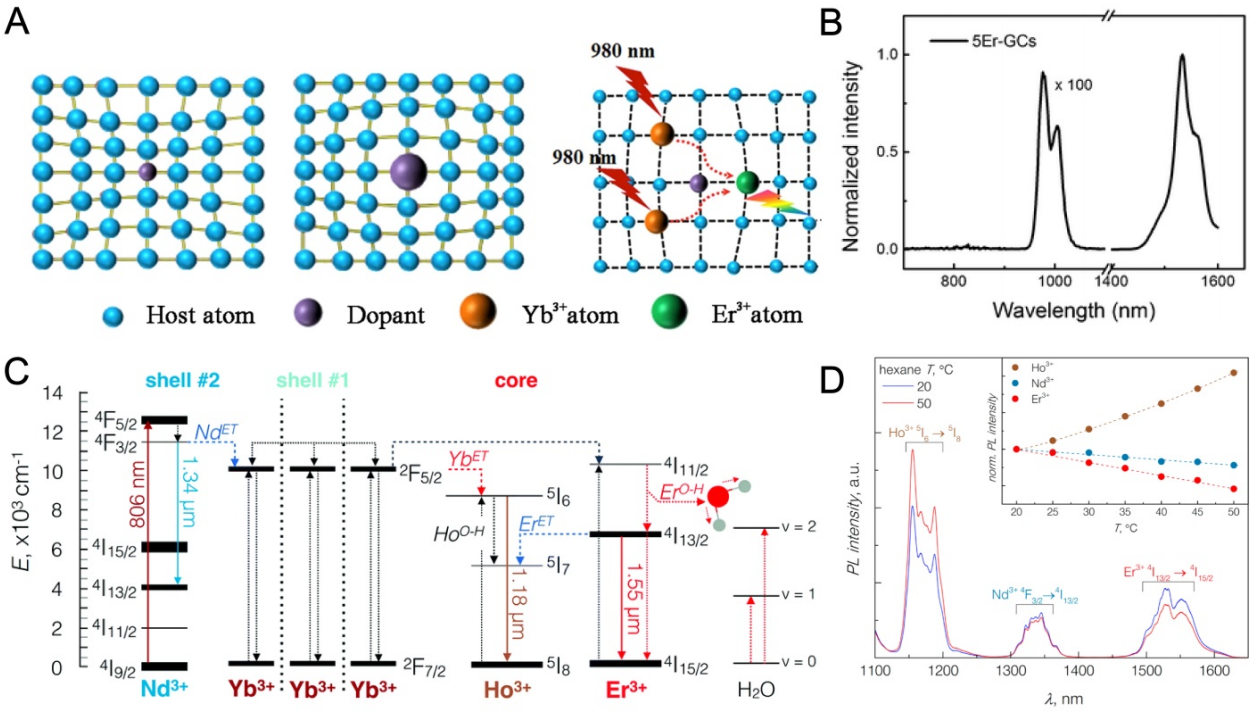

Figure 2. Luminescence mechanism of RE nanoparticles. (**A**) Scheme of emission mechanism of Yb, Er doped RE nanoparticles exited by 980 nm NIR light. Adapted with permission from [83], Copyright 2018, Nature Springer. (**B**) NIR-spectra of 5% Er^{3+} doped glass ceramics upon 400 nm irradiation. Adapted with permission from [84], Copyright 2015, Royal Society of Chemistry. (**C**) Principal operation scheme for the NIR-to-NIR emission of RE doped nanoparticles. (**D**) NIR emission bands of Ho^{3+} (1.18 μm), Nd^{3+} (1.34 μm), and Er^{3+} (1.55 μm) ions excited with 806 nm irradiation. Adapted with permission from [85], Copyright 2017, Royal Society of Chemistry.

Due to the involvement of multiple steps in one single luminescence process, including electron transition and the transition probability (Figure 2a), the excitation selection, multiphonon relaxation and energy transfer, Stokes shift and line broadening,[86] the study of RE nanoparticle emission is highly confusing where lots of details remains unclear. For example, at least 6 states were involved in an Yb, Er, Nd-co-doped triple-layered core-shell NIR fluorophore [84]. During the absorption process of 800 nm light, the $^4I_{9/2}\rightarrow{}^4F_{5/2}$ transition of Nd^{3+} is firstly involved. After that, the energy is fast transferred to the inner layer by a $^2F_{7/2}\rightarrow{}^2F_{5/2}$ process between Nd^{3+} and Yb^{3+}. Consequent energy transfer happens by the co-doped Yb^{3+} and then sensitize Er^{3+} ($Yb^{3+}\rightarrow Er^{3+}$, $^4I_{15/2}\rightarrow{}^4I_{11/2}$). After all, the relaxation from the excited state of Er^{3+} finally releases a 1525 nm ($^4I_{13/2}\rightarrow{}^4I_{15/2}$) photon *via* phonon vibration process (Figure 2b). Similarly, a complicated phonon-assisted Yb^{3+} ($^2F_{5/2}$) → Ho^{3+} ($^5I_6$) and Nd^{3+} ($^4F_{3/2}$) → Yb^{3+} ($^2F_{5/2}$) energy transfer mechanism was proposed in Yb^{3+}, Ho^{3+}, Nd^{3+} doped core/shell $NaGdF_4$ nanoparticles and it was designed as a nanothermometer due to a temperature-dependent promotion of the electronic-to-vibrational energy transfer (Figure 2c,d). Steady/transient state fluorescence spectroscopy, fluorescence polarization spectroscopy, and femto-second laser pulse luminescence etc. were widely used to study the emission mechanisms of RE fluorophores [87,88]. The better understanding of the luminescence mechanism will help to design better NIR probes as well as further broadened applications.

2.2. Material Subclasses of NIR emissive RE nanoparticles

RE oxides [89,90], in most cases, Y_2O_3, (Figure 3a) is the first generation NIR emissive lanthanide material [91,92]. In a typical synthesis of RE oxides, the nanoparticles were synthesized through homogeneous precipitation and then high temperature calcination is required to increase the emission efficiency if necessary. In 2003, Vetrone and his coworkers investigated the upconversion emission of nanocrystalline and bulk Y_2O_3:Er^{3+} and the influence of the erbium concentration to the luminescence [93]. They reported that by adjusting the doping concentration, a transition in emission from visible to NIR region was observed. Soga group further developed liposome encapsulated, Er-doped Y_2O_3 nanoparticles with various surface modifications as a fluorescent probe for NIR bioimaging [90]. The authors introduced PEG on the liposome surface to avoid nonspecific interaction with proteins. Both microscopic and macroscopic NIR imaging systems were applied to image the organs of a mouse injected with the NIR-encapsulated liposomes as a demonstration of successful NIR bioimaging. But limited by the relatively low NIR emission efficiency

of lanthanide oxides, their applications stop at organ bioimaging and no more clinical approaches were conducted.

RE fluorides [94,95], referring to YF_3 and LaF_3, [96] and maybe more frequently, $NaYF_4$ and $NaGdF_4$ [73,87], were the most widely used doping matrices (Figure 3c) for lanthanide phosphor [79]. This is largely because $NaLnF_4$ exhibits the lowest non-radiative energy loss and endow the highest quantum yield for a major of lanthanides doping. The $NaLnF_4$ is still the most widely used matrix [97] for NIR emission through either upconversion or downshifting luminescence by different rare earth doping, largely on account to the high emission efficiency and extraordinary chemical stability. In addition, $NaGdF_4$ also has excellent magnetic properties and it was widely employed as contrast agents in MRI [98,99]. The classic synthesis of $NaYF_4$ or $NaGdF_4$ nanoparticles was conducted in oleic acid and 1-octadecene through a solvothermal method, using lanthanide nitric salts or lanthanides acetates, reacting with NaF or NH_4F. The versatile luminescent properties as well their intriguing magnetic and electronic properties of RE fluorides open an avenue to multi-mode molecular imaging and dual signal guided surgery [100]. For example, Riman's group prepared highly NIR emissive fluoride nanopowders (LaF_3: Nd and CaF_2: Er) with solvothermal methods (Figure 3b). The quantum efficiencies were as high as 95% for LaF_3: Nd and 51% for CaF_2: Er, which are much higher than RE oxides [94]. In 2013, Zhou *et al.* employed Tm and Nd doped NaGdF4 nanoparticles to efficient NIR-to-NIR upconversion and down-shifting emission, providing a dual mode platform for NIR fluorescence bioimaging and promisingly even magnetic resonance imaging (MRI) probes [69].

Recently, a series of new matrices were reported for NIR emission of lanthanides [80,103,104], where solid state high-temperature synthesis were usually employed. The new matrices bring new properties to NIR based bioimaging, such as long persistence emissive phenomenon and degradability in physiological fluids. For example, Scherman *et al.* reported to successfully prepare lanthanide doped $Ca_{0.2}Zn_{0.9}Mg_{0.9}Si_2O_6$ nanoparticles with NIR persistent luminescence [82]. The NIR persistent nanoparticles can be excited before injection to mouse, and the biodistribution of the nanoparticle can be monitored in real-time for more than 1 h without any external illumination source. The nanoparticles were modified with targeting ligands, would guide the nanoparticles specifically to lung, liver or to long-lasting blood circulation. This system can be employed to evaluate tumor mass and showed great clinical potential. Another similar work was reported by Yan's lab that they synthesized NIR emitting $Zn_{2.94}Ga_{1.96}Ge_2O_{10}$ nanoparticles co-doped with Cr^{3+}, Pr^{3+} for long persistent luminescence (Figure 3d). The nanoprobe was further functionalized with gadolinium complexes and enabled a multimodal *in vivo* MRI and NIR luminescence imaging [102].

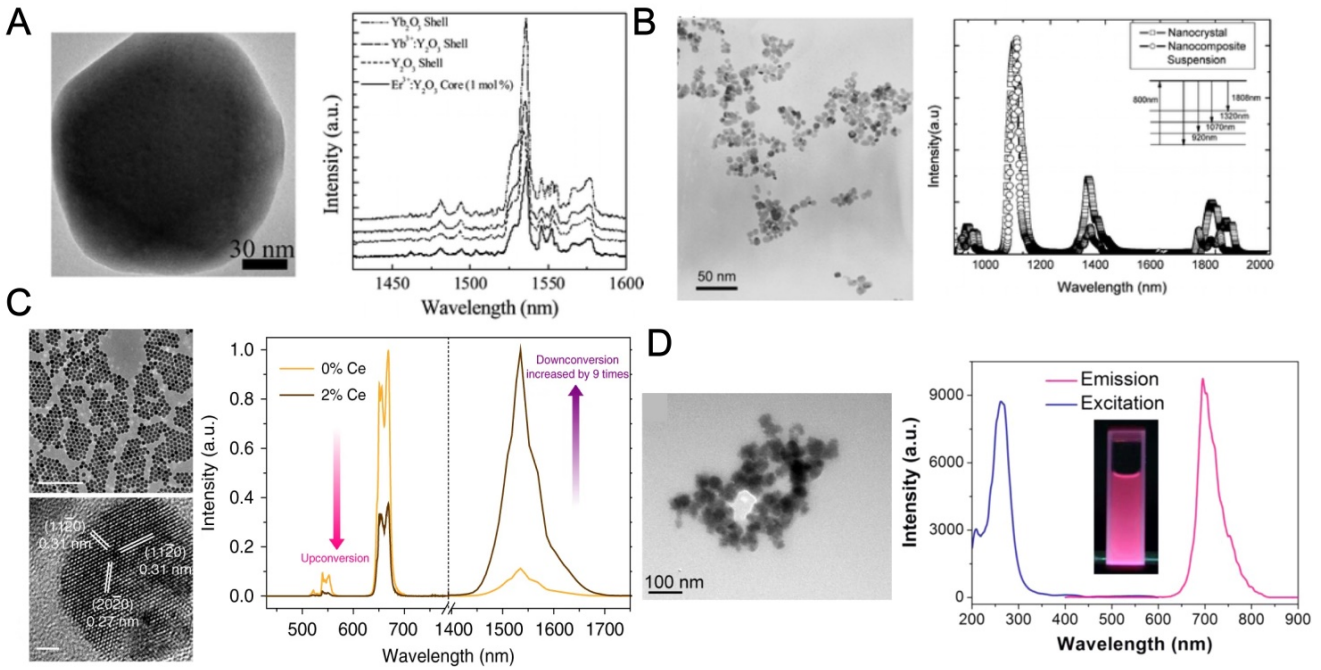

Figure 3. Subclasses of RE nanoparticles. TEM images (left) and NIR fluorescent spectra of (**A**) Yb_2O_3 nanoparticles, adapted with permission from [91], Copyright 2012, American Chemical Society. (**B**) YF_3 nanoparticles, adapted with permission from [94], Copyright 2007, American Chemical Society. (**C**) $NaYF_4$ nanoparticles, adapted with permission from [101], Copyright 2017, Nature Springer and (**D**) $Zn_{2.94}Ga_{1.96}Ge_2O_{10}$ nanoparticles, adapted with permission from [102], Copyright 2014, American Chemical Society.

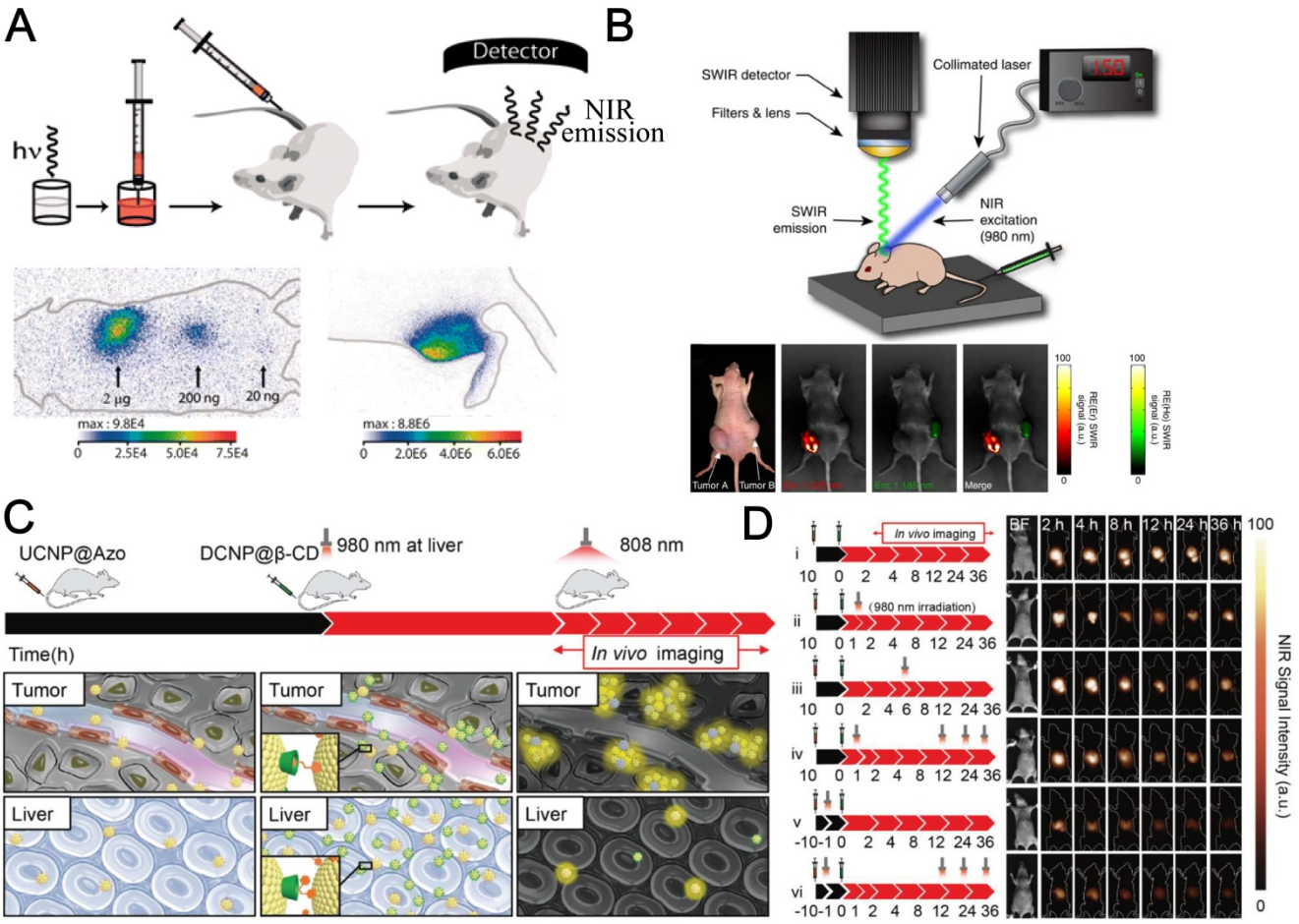

Figure 4. RE nanoprobes for NIR bioimaging *in vivo*. (**A**). Principal scheme for *in vivo* experiments and NIR bioimaging. NIR images of mice at different localizations with different nanoparticle amounts. Adapted with permission from [82], Copyright 2007, National Academy of Sciences. (**B**). Schematic of the portable short-wave infrared (SWIR) imaging prototype using 980 nm NIR excitation and the bioimaging for injected tumor on nude mouse. Adapted with permission from [114], Copyright 2013, Nature Springer. (**C**) Scheme illustration of assembly and NIR laser-regulated disassembly of nanoprobes for stable and accurate NIR-II bioimaging. (**D**) Schematic depiction of experimental timeline for the *in vivo* assembly and 980 nm laser-triggered *in vivo* disassembly and NIR-II fluorescence bioimaging results for the abdomen (1000 nm long-pass filter) of the nude mice with murine epidermal tumor by two-staged in-sequence injection of RE nanoparticles (interval between two injections is 10 h) under 808 nm excitation. Adapted with permission from [115], Copyright 2018, John Wiley & Sons, Inc.

3. RE nanoparticles for NIR bioimaging

Fluorescence based bioimaging in the NIR window features deep tissue penetration, reduced tissue scattering, and decreased tissue autofluorescence. These advantages would largely improve the performance of nanoparticles in biological and pre-clinical applications. Hence, NIR fluorescent probes, especially RE nanoparticles, are constructed into platforms for NIR bioimaging [105], biosensing [106], drug delivery [107], photodynamic therapy and NIR based IGS [108]. The application in bioimaging is the first step for successive preclinical studies and practices. The good performance in NIR bioimaging of RE nanoparticles plays as cornerstones for the follow-up photodynamic therapy, drug delivery and surgical navigation.

Various groups have successfully reported NIR emissive RE nanoparticles for bioimaging [109] (Figure 4a). Hammond's group constructed LbL-modified NIR-II nanoparticels from RE doped $NaYF_4$ fluorescent materials to perform a side-by-side investigation and comparison for the biodistribution, pharmacokinetics, and toxicities of these probes [110]. Moghe *et al.* reported a multispectral, real-time short-wavelength infrared imaging offering anatomical resolution using brightly emitting RE nanomaterials and demonstrate their practicability as a disease-targeted imaging method (Figure 4b) [111]. RE nanomaterials modified with human serum albumin (HSA) endowed systemic study of biodistribution of the RE nanoparticles. It was reported by the authors that accumulation and retention in tumor tissue was improved after protein conjugation, which was visualized by the localized enhancement of NIR signal intensity (Figure 4b). The involvement of HSA was drawn as experiences by a lot of other studies and was verified to improve the biocapability and retention time in organs and tumors [112]. Liu's group found another route of NIR

emitting nanomaterials for theranostic applications on how RE moieties were involved. They fabricated a nanocomplex where Gd^{3+} chelate were functionalized onto HSA, conjugated with a NIR dye IR825 [113]. The albumin-based probe was capable of multimodal imaging and photothermal therapy (PTT). The authors also validated the practicability of an NIR 'photothermal ablation assisted surgery' strategy using the theranostic nanoassay, which is promising for future clinical cancer treatment.

In 2019, a surge of RE nanoparticles for NIR bioimaging have been reported by different research groups. Zhang's group reported that *in vivo* assembly and disassembly of supramolecularly engineered NIR-II emissive RE nanoparticles (Figure 4 c,d) can greatly improve the quality of bioimaging [115]. In another work by the same team, they succeeded in precise *in vivo* inflammation imaging technique using *in situ* responsive cross-linking of glutathione-modified NIR-II lanthanide nanoparticles. NIR-II signals in the inflamed area were observed within 10 min and lasted as long as 8 h. The signal-noise ratio of inflammatory bioimaging was enhanced 2.9-fold compared with reference groups at the same time. Their ROS-responsive *in vivo* crosslinking strategy provides a safe and easy route for the fast location of and long-term imaging of inflamed areas [116]. Li et al. proposed the poly(acrylic acid) (PAA)-modified $NaLnF_4$:40Gd/20Yb/2Er nanorods (Ln = Y, Yb, Lu, PAA-Ln-NRs) with enhanced downshifting NIR-IIb emission for improved quality of bioimaging [117]. The downshifting emission beyond 1500 nm is doubled by suppressing the upconversion path through Ce^{3+} doping. The explored bright NIR-IIb emitted PAA-Lu-NRs were used for a series of applications, including high sensitivity small tumor (~4 mm) imaging, metastatic tiny tumor detection (~3 mm), high spatial resolution (41 μm) tumor vessel visualization, and brain vessel imaging. Their findings opened the opportunity of utilizing the RE based NIR-IIb probe for *in vivo* tumor vessel/metastasis and noninvasive brain vascular imaging. It should be drawn more interests that Gu et al. reported an important progress of NIR bioimaging using RE nanoparticles [118]. In their work, a time-domain (τ) based light transducer was applied instead of conventional spectra-domain signaling, serving as a new weapon for *in vivo* NIR imaging. The ytterbium-based transducer can convert the pulsed NIR irradiation into long-decaying luminescence with an efficiency approaching 100%. This technique can largely improve the signal-to-noise ratio and bioimaging quality in mice models.

DNA nanotechnology [119] also plays an important role in bioimaging using RE nanoparticles. DNA structures, including G-quadruplexes [120], aptamers [121], molecular switches [122], framework nucleic acids [123] (FNAs, eg. DNA tetrahedrons [124,125]), and origamis [126], were widely involved in design of probes for RE nanoparticles based bioimaging systems [127] or theranostic devices [128,129]. In comparison of other materials such as inorganic gold nanoparticles [130,131], DNA nanostructures [132,133] showed extraordinary biocompatibility, degradability, low size dispersibility [134] and programmability [135]. The reversible Watson-Crick pairing of DNA also provide a versatile platform to construct dynamic, programmable, precisely controlled devices [136] for sensing [137] and imaging in combination of RE nanoparticles. For example, Lu and his group introduced DNA modifications to RE nanoparticles and successfully obtained controllable assemblies of gold nanoparticles onto RE upconversion nanoparticles for improved drug delivery and bioimaging [138]. Kuang *et al.* reported the self-assemblies of RE nanoparticles with DNA tetrahedrons and applied them as a chiral sensing platform for cell imaging and direct observation of autophagy [139].

4. RE nanoparticles for NIR photodynamic therapy (PDT) and drug delivery

The NIR bioimaging systems were widely studied in various biological applications and clinical attempts, such as cell and tissue imaging, tumour diagnosis and therapy, and surgical navigation. However, limited by the difficulties of clinical practices, most of the researches of NIR bioimaging did not reach the surgical guidance level. Considering this, we also concluded the recent progresses in photodynamic therapy (PDT) and drug delivery using rare earth nanoparticles since the requirements of the probes and the NIR imaging equipment are similar with IGS but practically much easier to achieve to a lot of research groups in this field. The highly related fields will share a view in material design, safety estimation, animal models and so on [140]. For bioimaging and IGS applications, the performance is largely determined by the signal-to-background ratio and targeting affinity. It requires higher fluorescence efficiency, lower tissue photo-absorption and stabilized functionalization. Down-shifting RE nanoparticles with NIR-II emission excited by NIR-I laser is commonly used to achieve good *in vivo* bioimaging quality. For PDT and drug delivery design, higher photon energy is demanded to trigger the ROS generation or release of cargos. And upconversion nanoparticles that will give rise to the photon energies are preferred.

Photodynamic therapy (PDT) is a non-invasive treatment modality for a variety of diseases including cancer [141,142]. A recent popular strategy to conduct PDT is based on a subclass of RE nanoparticles, upconversion nanoparticles (UCNPs). Upon NIR excitation, UCNPs emit visible light with anti-Stokes shifts, which can be applied to activate modified photosensitizers to produce reactive oxygen species (such as $^1O_2$) and damage cancer cells through oxidative stress and activated metabolic autophagy [143]. NIR-excited UCNPs can be utilized to activate photosensitizers in deep tissues and exhibit wider coverage of therapies and better efficiency than traditional PDT under visible or UV light illumination. Similarly, RE nanoparticles could also be used for NIR light-triggered drug release [144] through photothermal process or photochemical cascade reactions [145,146].

The first *in vivo* UCNP-based PDT study on animals was demonstrated by Liu's team. [48] They applied non-covalently incorporated Ce6 onto PEGylated amphiphilic polymer-coated upconversion nanoparticles (UCNPs). The obtained UCNP-Ce6 complex could enter cancer cells and induce 4T1 cell death after being exposed to the 980-nm NIR light. The survival of mice after UCNP-Ce6 injection and PDT treatment was dramatically pro-longed compared to the control group. They also found that the injected UCNPs could be gradually cleared out after 2 months, determined by *ex vivo* ICP-AES measurement, without noticeable toxicity to the treated mice. It is valuable that the authors also compared the tissue penetration abilities for the same NIR probes induced by 980-nm NIR light and 660 nm visible light. It is observed that more singlet oxygens were generated under 660-nm illumination, in comparison to UCNP-Ce6 sample under the 980 nm excitation. But under 8 mm tissue (pork) blocking, 660 nm visible light will lose its power in singlet oxygen production but 980 nm NIR illumination remains high efficiency. Very recently, Yu et al. developed a pre-protective strategy using a switchable folic acid modified UCNPs conjugated with two types of DNA in different lengths. In normal tissues, folic acid is protected by longer DNA. The platform can be triggered in tumor site to exposed folic acids for tumor targeting and NIR PDT (Figure 5a) [147].

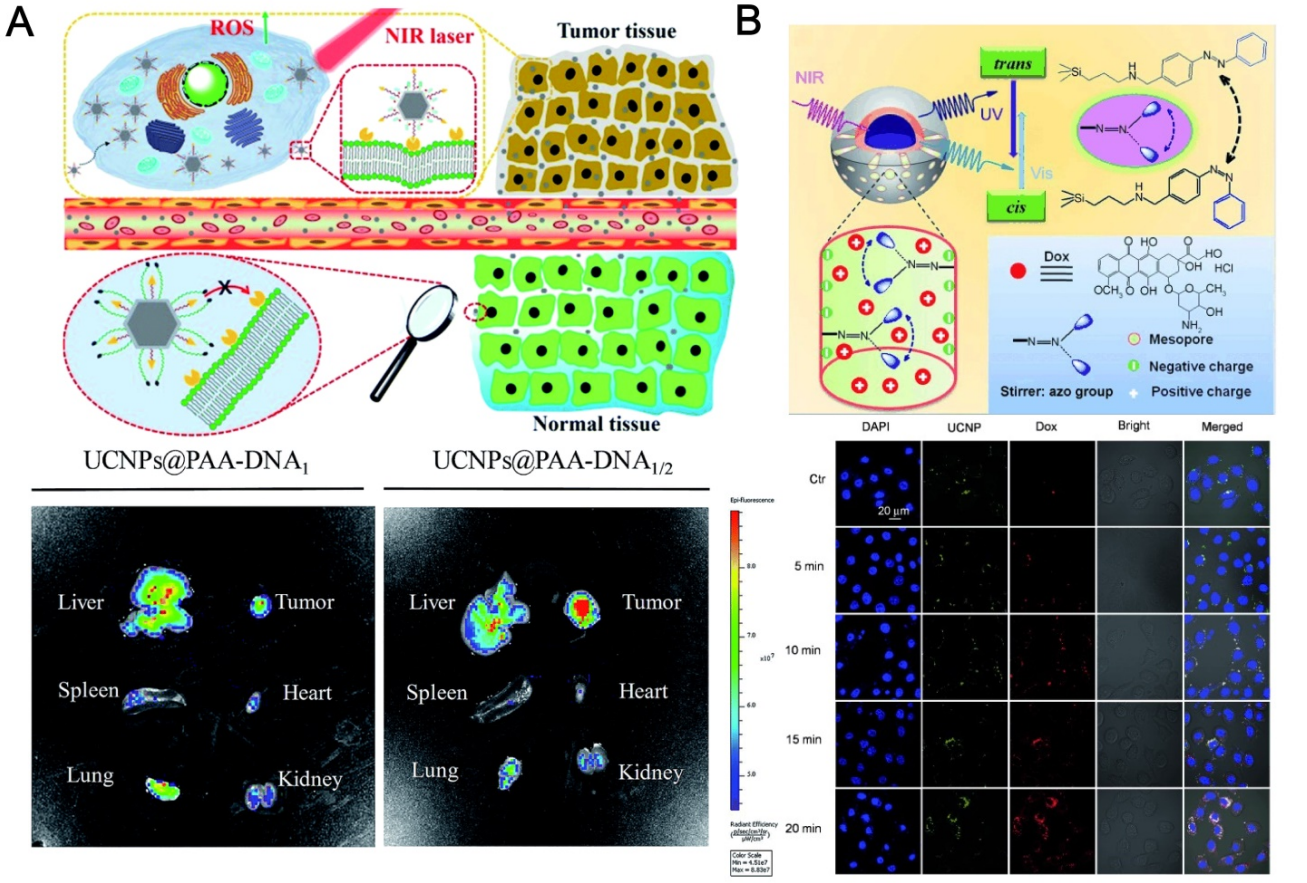

Figure 5. (**A**) Precise tumor targeting and specific PDT for cancer of UCNPs@PAA-DNA. *In vivo* imaging of five major organs harvested from a mouse at 8 h postinjection with UCNPs@PAA-DNA1(Ce6) (left) or UCNPs@PAA-DNA1/2 (right). Adapted with permission from [147], Copyright 2018, Royal Society of Chemistry. (**B**) Upper: NIR light-triggered Dox release by making use of the upconversion property of UCNPs and trans–cis photoisomerization of azo molecules grafted in the mesopore network of a mesoporous silica layer. Down: CLSM observations of the photocontrolled Dox release in HeLa cells. Adapted with permission from [145], Copyright 2013, John Wiley & Sons, Inc.

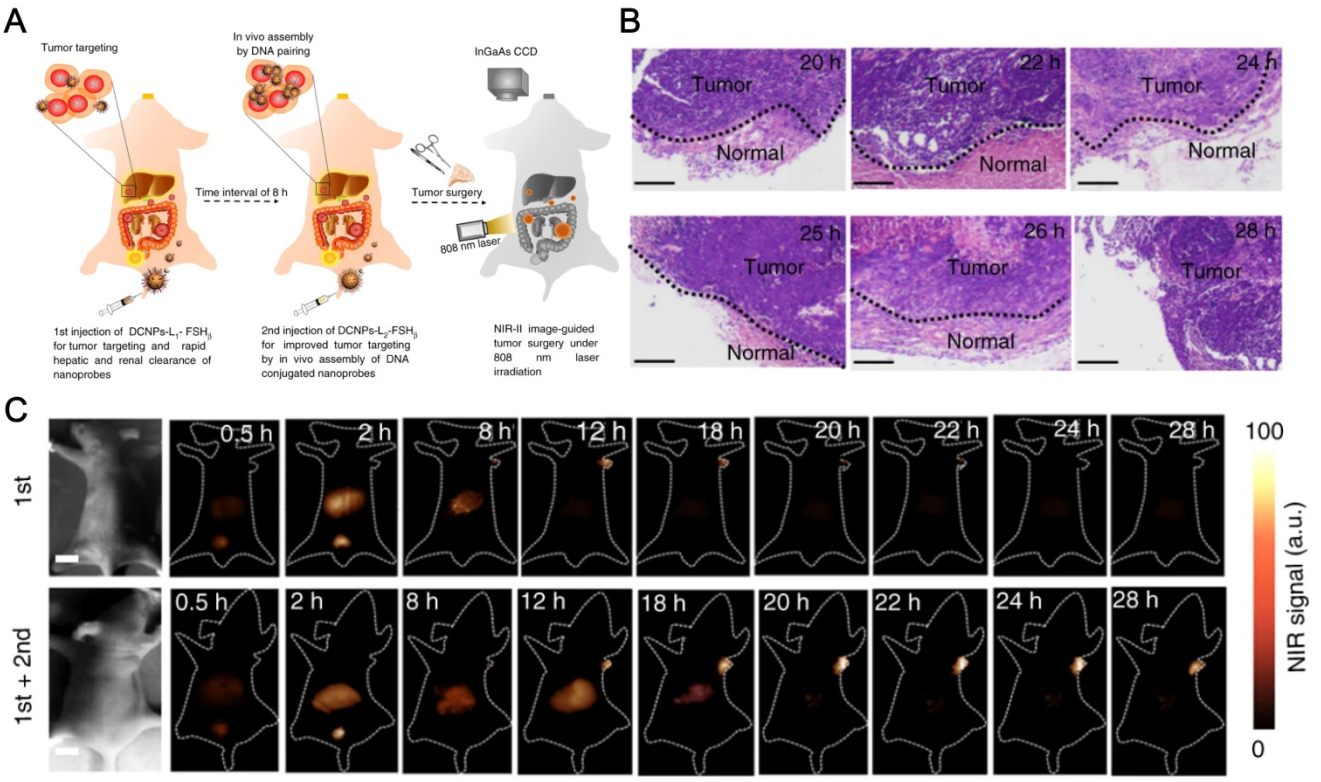

Figure 6. $NaGdF_4$ based NIR-II nanoprobes *in-vivo* assembly to improve IGS for metastatic ovarian cancer. (**A**) Schematic illustration of NIR-II nanoprobes fabrication for ovarian metastasis surgery under NIR-II bioimaging guidance. (**B**) Hematoxylin and eosin (H&E) staining results of the tumors resected in 20–28 h PI under NIR-II fluorescence bioimaging guidance. (**C**) NIR-II fluorescence bioimaging (1000 nm long-pass filter) of the nude mice with murine epidermal tumor by single caudal vein first injection and two-staged in sequence injection (first + second) (interval between two injection is 8 h) under 808 nm excitation (fluence rate = 40 mW cm^{-2}). The concentration of DCNPs in single injection is same to the sum of that for two-staged injection. All scale bars: 1 cm. Representative images are for n = 5 per group. Adapted with permission from [150], Copyright 2017, Nature Springer.

Besides the application of UCNPs in PDT, photo-responsive drug release systems using NIR triggering, have received remarkable emphasis in recent years, due to their promising potential in noninvasive theranostics at the site of nidus (*e.g.* tumors) [148]. For example, Shi *et al.* fabricated mesoporous silica coated UCNPs modified by azobenzene molecules. [145] The anticancer drug doxorubicin (DOX) were controllably released from the outer layer of the mesoporous silica under NIR laser irradiation (Figure 5b). Qu *et al*. reported a NIR upconversion responsive system carrying two cargos (clioquinol and curcumin) to stepwise sequential release [149]. When the UCNP platform is irradiated at low intensity of the NIR laser, clioquinol is first released for chelating with free metal ions such as Cu^{2+}, which hinders the efficacy of curcumin. Subsequently, under higher intensity of NIR illumination, curcumin is subsequently released. The stepwise-release strategy can greatly improve the activity of curcumin for the inhibition of amyloid aggregation. Excess Cu^{2+} ions and superfluous ROS can be cleaned up by the NIR-triggered drug delivery platform.

5. Surgery guide using NIR emissive RE nanoparticles

Inspired by the success of bioimaging and PDT therapies using NIR emissive nanoparticles, researchers urged to put forwards the employment of NIR probes into clinical practices. Tian *et al.* used $ZnGa_2O_4Cr_{0.004}$ (ZGC) nanoparticles for guided surgery during operation to accurate delineation of hepatocellular carcinoma (HCC) [23]. ZGC showed excellent long-lasting NIR afterglow properties that lasted for hours, which can improve real-time guided surgical quality. Though the ZGC nanoparticles employed in this work were not consisting of any RE elements, the ZGC probes with NIR emission is surely a continuum of its prototype counterpart--$Zn_{2.94}Ga_{1.96}Ge_2O_{10}:Cr^{3+},Pr^{3+}$ nanoparticles, where RE element Pr plays as emitters [80].

Very recently, Zhang's lab at Fudan University also reported *in vivo* assembly of the lanthanides doped $NaGdF_4$ based NIR-II emitting nanoparticles to improve the IGS for metastatic ovarian cancer (Figure 6) [150]. The NIR-II probes were modified with DNA and targeting peptides while the imaging quality is largely improved with good photostability and deep tissue penetration over 8 mm, in comparison to that of

conventional organic dye, indocyanine green (ICG). The authors observed *in vivo* assembly of the nanoprobes, which increases the tumor retention period to 6 h, enabled precise tumor resection. Also, better tumor-to-normal tissue ratio is successfully achieved to facilitate the abdominal ovarian metastases surgical operation. The preclinical practice proved that metastases smaller than 1 mm can be completely excised under Zhang's NIR-II bioimaging guidance. This work is a milestone of the applications of RE based NIR emissive nanoparticles and greatly encourages researchers to bring NIR fluorescence IGS to clinical surgery.

There is an increase of reports of NIR-II based IGS using RE nanoparticles since last year. Liu and his collaborators fabricated functionalized red blood cells with RE UCNPs as a multimodal probe for NIR-II luminescence guiding precise tumor resection under an 808-nm laser irradiation and meanwhile laser activated O_2 release to help PDT therapy for popliteal lymph node metastasis [152]. In their work, it is clearly shown that NIR-II fluorescence imaging largely improves the penetration of light and exhibits lower signal-noise ratio. The penetration depth of the NIR-II fluorescence of their probe doubled in comparison of that for NIR-I fluorescence. The red blood cell and RE nanoparticles based NIR-II probe enabled the successfully NIR-II guided surgical removal of small tumor with a size of 7 mm^3 and 3 mm^3 (Figure 7 b,c).

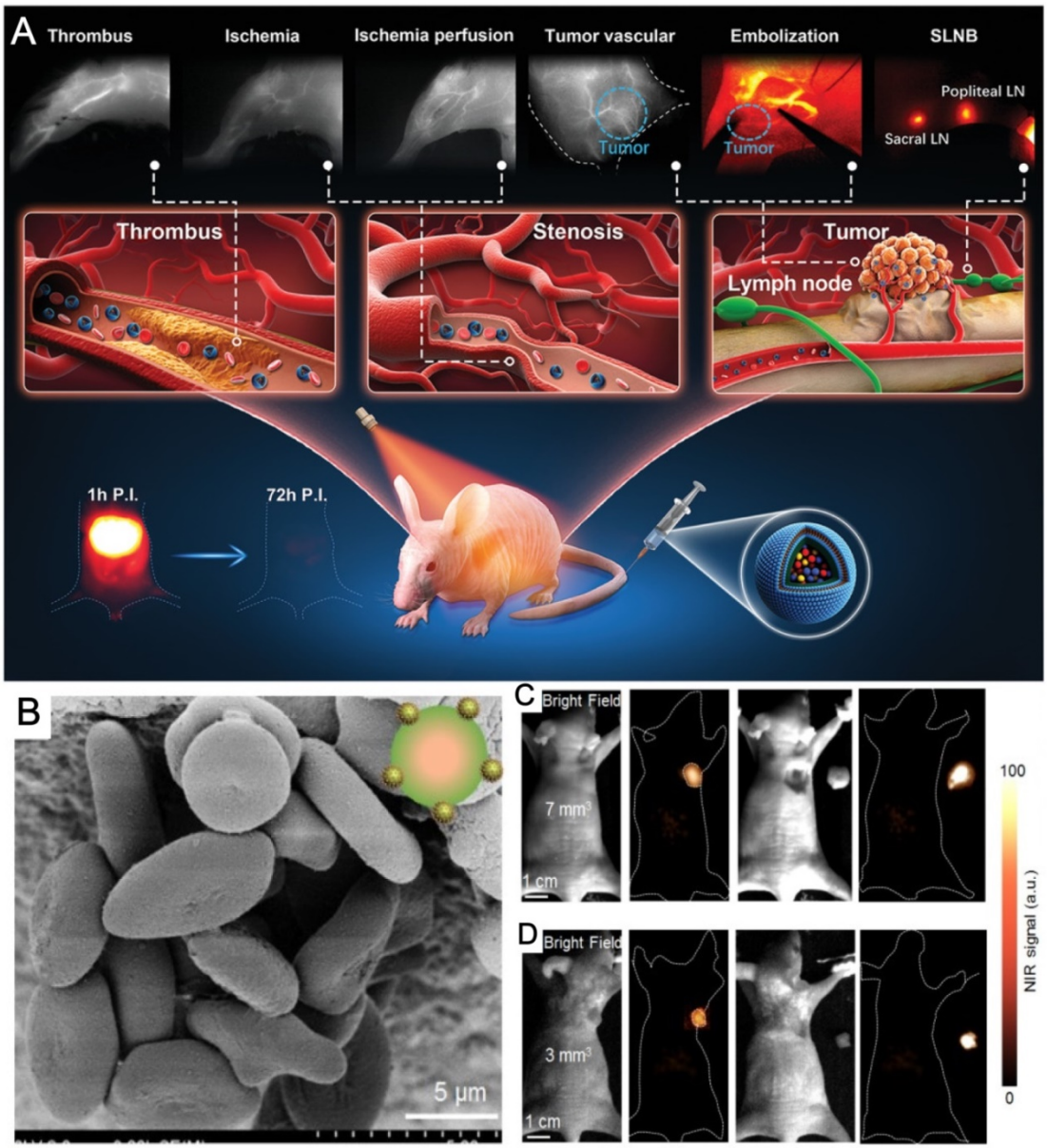

Figure 7. RE nanoparticles for surgical guidance with NIR imaging. (**A**) Schematic illustration of excretable RE nanoparticle for multifunctional biomedical imaging and ICG in the NIR-II window. (**B**) SEM images of multimodal probes enabled by red blood cell coated with NIR-II emissive lanthanide nanoparticles. Adapted with permission from [151], Copyright 2019, John Wiley & Sons, Inc. (**C, D**) NIR II fluorescence bioimaging results (12 h PI) of epidermal tumors with sizes of 7 mm^3 (**C**) and 3 mm^3 (**D**) and NIR II fluorescence bioimaging results after the surgical resection of tumors. Adapted with permission from [152], Copyright 2019, Ivyspring International Publisher.

All the above-mentioned reports of RE based NIR-bioimaging guided surgery concentrated on direct targeting to the tumor or immunological recognition of cancer tissues. However, Li *et al.* provided us another choice for NIR imaging based IGS with RE nanoparticles, without any targeting strategies to tumors [151]. The RE nanoparticles was used for NIR-II visualization of circulatory systems instead of the tumors. Due to the moderate half-time of blood circulation, their probes are capable of monitoring vascular disorders including artery thrombosis, ischemia, and tumor angiogenesis. The cancer therapy was constructed through a blood vessel embolization surgery conducted with NIR-II navigation of femur orthotopic osteosarcoma on nude mice. In addition, the NIR-II probe is also applicable for sentinel lymph nodes imaging and sequential biopsy by tail injection.

6. Conclusion and Perspective

Rare earth nanoparticles have many advantages, such as high NIR luminescence efficiency, low toxicity, and good biocompatibility. They hold great promise in a wide range of applications in cancer diagnosis and treatment, and surgical navigation. However, there are only limited reports on the application of RE nanoparticles in surgical navigation at clinical level. NIR small molecular dyes and quantum dots are still the mainstream of probes for NIR fluorescence ICG. This is mainly because of the following two reasons: 1) Concerns about the safety of RE nanoparticles, including their refractoriness and toxicity of possibly released rare earth ions; 2) In order to achieve higher sensitivity and spatiotemporal resolution in IGS, smaller RE nanoparticles are required, however, the luminescence efficiency of RE nanoparticles decreases rapidly within smaller size nanoparticles [153]. Whereas the nanoparticles smaller than 10 nm has no advantage against competing semiconductor quantum dots in terms of luminescence efficiency.

On the other hand, the current reports of NIR surgical navigations using lanthanide nanoparticles are mostly focused on simple animal models such as ovarian tumor metastases and unilateral thrombus on nude mice. Larger animals such as rabbits [154] and dogs [155] have not yet been employed in NIR emissive RE nanoparticles based IGS. Considering that the major advantage of using NIR emissive RE nanoparticles is to boost the penetration depth of the excitation light, it is important to verify it in larger animals with thicker tissues. Thus, it is of great urgency to develop new disease models to larger mammals which can be better mimics for human body. However, the penetration depth of NIR fluorescence of current reports are mostly no larger than 10 mm, which is obviously impractical for clinical surgery of human body. From this aspect, we shall prospect that there is still great space for the improvement of the fluorescence intensity, quantum yield, noise-to-background ratio and eventually penetration depth for the RE nanoparticles of NIR emission.

Therefore, the future development trends of RE nanoparticles in the field of NIR fluorescent IGS are proposed as follows: a) Develop degradable and metabolizable rare earth nanoparticles, where the metabolites of the nanoparticles are required to be non-toxic too; b) Further improve the luminescence efficiency of NIR, especially for small size nanoparticles, it is necessary to surpass inorganic semiconductor quantum dots (such as Ag_2S) [156] and also improve the penetration depth of NIR fluorescence. c) Expand the unique luminescent properties such as long afterglow and time-resolved luminescence, and utilize the magnetism of rare earth elements such as gadolinium to develop multi-mode molecular imaging technology including MRI and multiple optical imaging techniques.

Acknowledgments

This work was supported by the National Science Foundation of China (21834007, 21904087), National Key R&D Program of China (2016YF A0400900), Science and Technology Commission of Shanghai Municipality (19ZR1474600), China Postdoctoral Science Foundation (2018M641995), the Key Research Program of Frontier Sciences (QYZDJ-SSW-SLH031), the Open Large Infrastructure Research of CAS, Chinese Academy of Sciences, LU Jiaxi International Team of the Chinese Academy of Sciences, K. C. Wong Foundation at Shanghai Jiao Tong University, and Innovative research team of high-level local universities in Shanghai.

Competing Interests

The authors have declared that no competing interest exists.

References

1. Demicheli R, Retsky MW, Hrushesky WJM, Baum M, Gukas ID. The effects of surgery on tumor growth: a century of investigations. Ann Oncol. 2008; 19: 1821-8.
2. de Boer E, Harlaar NJ, Taruttis A, et al. Optical innovations in surgery. Brit J Surg. 2015; 102: e56–72.
3. Cabioglu N, Hunt KK, Sahin AA, et al. Role for Intraoperative Margin Assessment in Patients Undergoing Breast-Conserving Surgery. Ann Surg Oncol. 2007; 14: 1458–71.
4. Weatherall PT, Evans GF, Metzger GJ, Saborrian MH, Leitch AM. MRI vs. histologic measurement of breast cancer following chemotherapy: Comparison with x-ray mammography and palpation. J Magn Reson Imaging. 2001; 13: 868–75.

5. Debie P, Hernot S. Emerging Fluorescent Molecular Tracers to Guide Intra-Operative Surgical Decision-Making. Front Pharmacol. 2019; 10: 510-20.
6. Yang L, Sajja HK, Cao Z, et al. uPAR-targeted optical imaging contrasts as theranostic agents for tumor margin detection. Theranostics. 2013; 4: 106-18.
7. Nagao T, Inoue S, Yoshimi F, et al. Postoperative recurrence of hepatocellular carcinoma. Ann Surg. 1990; 211: 28-33.
8. Zou L, Wang H, He B, et al. Current Approaches of Photothermal Therapy in Treating Cancer Metastasis with Nanotherapeutics. Theranostics. 2016; 6: 762–72.
9. Homann M, Sansjofre P, Van Zuilen M, et al. Microbial life and biogeochemical cycling on land 3,220 million years ago. Nat Geosci. 2018; 11: 665–71.
10. Sun Y, Ding F, Zhou Z, et al. Rhomboidal Pt(II) metallacycle-based NIR-II theranostic nanoprobe for tumor diagnosis and image-guided therapy. Proc Natl Acad Sci. 2019; 116: 1968-1973.
11. Chi C, Du Y, Ye J, et al. Intraoperative imaging-guided cancer surgery: from current fluorescence molecular imaging methods to future multi-modality imaging technology. Theranostics. 2014; 4: 1072–84.
12. Gu K, Xu Y, Li H, et al. Real-Time Tracking and *In Vivo* Visualization of β-Galactosidase Activity in Colorectal Tumor with a Ratiometric Near-Infrared Fluorescent Probe. J Am Chem Soc. 2016; 138: 5334–40.
13. Zhou Y, Wang D, Zhang Y, et al. A Phosphorus Phthalocyanine Formulation with Intense Absorbance at 1000 nm for Deep Optical Imaging. Theranostics. 2016; 6: 688–97.
14. Wu X, Sun X, Guo Z, et al. *In Vivo* and *in Situ* Tracking Cancer Chemotherapy by Highly Photostable NIR Fluorescent Theranostic Prodrug. J Am Chem Soc. 2014; 136: 3579–88.
15. Lv G, Guo W, Zhang W, et al. Near-Infrared Emission CuInS/ZnS Quantum Dots: All-in-One Theranostic Nanomedicines with Intrinsic Fluorescence/Photoacoustic Imaging for Tumor Phototherapy. ACS Nano. 2016; 10: 9637–45.
16. Wang C, Fan W, Zhang Z, Wen Y, Xiong L, Chen X. Advanced Nanotechnology Leading the Way to Multimodal Imaging-Guided Precision Surgical Therapy. Adv Mater. 2019; 0: 1904329. in press. doi: 10.1002/adma.201904329
17. Vahrmeijer AL, Hutteman M, Van Der Vorst JR, Van De Velde CJH, Frangioni J V. Image-guided cancer surgery using near-infrared fluorescence. Nat Rev Clin Oncol. 2013; 10: 507–18.
18. Low PS, Singhal S, Srinivasarao M. Fluorescence-guided surgery of cancer: applications, tools and perspectives. Curr Opin Chem Biol. 2018; 45: 64–72.
19. Chen G, Tian F, Zhang Y, Zhang Y, Li C, Wang Q. Tracking of Transplanted Human Mesenchymal Stem Cells in Living Mice using Near-Infrared Ag2S Quantum Dots. Adv Funct Mater. 2014; 24: 2481–8.
20. Kelderhouse LE, Chelvam V, Wayua C, et al. Development of tumor-targeted near infrared probes for fluorescence guided surgery. Bioconjug Chem. 2013; 24: 1075–80.
21. Mahalingam SM, Chu H, Liu X, Leamon CP, Low PS. Carbonic Anhydrase IX-Targeted Near-Infrared Dye for Fluorescence Imaging of Hypoxic Tumors. Bioconjug Chem. 2018; 29: 3320–31.
22. Wang H, Li X, Tse BW-C, et al. Indocyanine green-incorporating nanoparticles for cancer theranostics. Theranostics. 2018; 8: 1227–42.
23. Ai T, Shang W, Yan H, et al. Near infrared-emitting persistent luminescent nanoparticles for Hepatocellular Carcinoma imaging and luminescence-guided surgery. Biomaterials. 2018; 167: 216–25.
24. Deng H, Zhong Y, Du M, et al. Theranostic self-assembly structure of gold nanoparticles for NIR photothermal therapy and X-Ray computed tomography imaging. Theranostics. 2014; 4: 904–18.
25. Pal K, Sharma V, Sahoo D, Kapuria N, Koner AL. Large Stokes-shifted NIR-emission from nanospace-induced aggregation of perylenemonoimide-doped polymer nanoparticles: imaging of folate receptor expression. Chem Commun. 2018; 54: 523–6.
26. Palner M, Pu K, Shao S, Rao J. Semiconducting Polymer Nanoparticles with Persistent Near-Infrared Luminescence for *in Vivo* Optical Imaging. Angew Chem Int Ed. 2015; 54: 11477–80.
27. Zhang M, Yue J, Cui R, et al. Bright quantum dots emitting at ~1,600 nm in the NIR-IIb window for deep tissue fluorescence imaging. Proc Natl Acad Sci. 2018; 115: 6590 – 6595.
28. Kim S, Lim YT, Soltesz EG, et al. Near-infrared fluorescent type II quantum dots for sentinel lymph node mapping. Nat Biotechnol. 2004; 22: 93–7.
29. Zhu S, Yung BC, Chandra S, Niu G, Antaris AL, Chen X. Near-Infrared-II (NIR-II) Bioimaging via Off-Peak NIR-I Fluorescence Emission. Theranostics. 2018; 8: 4141–51.
30. Vivero-Escoto JL, Huxford-Phillips RC, Lin W. Silica-based nanoprobes for biomedical imaging and theranostic applications. Chem Soc Rev. 2012; 41: 2673–85.
31. Martinho O, Silva-Oliveira R, Cury FP, et al. HER Family Receptors are Important Theranostic Biomarkers for Cervical Cancer: Blocking Glucose Metabolism Enhances the Therapeutic Effect of HER Inhibitors. Theranostics. 2017; 7: 717–32.
32. Weiler M, Dixon JB. Differential transport function of lymphatic vessels in the rat tail model and the long-term effects of Indocyanine Green as assessed with near-infrared imaging. Front Physiol. 2013; 4: 215-10.
33. Knapp DW, Adams LG, DeGrand AM, et al. Sentinel Lymph Node Mapping of Invasive Urinary Bladder Cancer in Animal Models Using Invisible Light. Eur Urol. 2007; 52: 1700–9.
34. Bergholt MS, Zheng W, Lin K, et al. Combining near-infrared-excited autofluorescence and Raman spectroscopy improves *in vivo* diagnosis of gastric cancer. Biosens Bioelectron. 2011; 26: 4104–10.
35. Keereweer S, Hutteman M, D.F. Kerrebijn J, J.H. van de Velde C, L. Vahrmeijer A, W.G.M. Lowik C. Translational Optical Imaging in Diagnosis and Treatment of Cancer. Current Pharmaceutical Biotech. 2012; 13: 498-503.
36. Hong G, Antaris AL, Dai H. Near-infrared fluorophores for biomedical imaging. Nat Biomed Eng. 2017; 1: 10-22.
37. Choi HS, Gibbs SL, Lee JH, et al. Targeted zwitterionic near-infrared fluorophores for improved optical imaging. Nat Biotechnol. 2013; 31: 148-53.
38. Li B, Lu L, Zhao M, Lei Z, Zhang F. An Efficient 1064 nm NIR-II Excitation Fluorescent Molecular Dye for Deep-Tissue High-Resolution Dynamic Bioimaging. Angew Chem Int Ed. 2018; 57: 7483–7.
39. He S, Song J, Qu J, Cheng Z. Crucial breakthrough of second near-infrared biological window fluorophores: Design and synthesis toward multimodal imaging and theranostics. Chem Soc Rev. 2018; 47: 4258–78.
40. Kam NWS, O'Connell M, Wisdom JA, Dai H. Carbon nanotubes as multifunctional biological transporters and near-infrared agents for selective cancer cell destruction. Proc Natl Acad Sci. 2005; 102: 11600–5.
41. Yang Q, Ma Z, Wang H, et al. Rational Design of Molecular Fluorophores for Biological Imaging in the NIR-II Window. Adv Mater. 2017; 29: 1605497-9.
42. Li Y, Bai G, Zeng S, Hao J. Theranostic Carbon Dots with Innovative NIR-II Emission for *in Vivo* Renal-Excreted Optical Imaging and Photothermal Therapy. ACS Appl Mater Interfaces. 2019; 11: 4737–44.
43. Bouzigues C, Gacoin T, Alexandrou A. Biological applications of rare-earth based nanoparticles. ACS Nano. 2011; 5: 8488–505.
44. Wang Y, Li Z, Hu D, Lin CT, Li J, Lin Y. Aptamer/graphene oxide nanocomplex for *in situ* molecular probing in living cells. J Am Chem Soc. 2010; 132: 9274–6.
45. Tian G, Gu Z, Liu X, et al. Facile Fabrication of Rare-Earth-Doped Gd2O3 Hollow Spheres with Upconversion Luminescence, Magnetic Resonance, and Drug Delivery Properties. J Phys Chem C. 2011; 115: 23790–6.
46. Gai S, Li C, Yang P, Lin J. Recent Progress in Rare Earth Micro/Nanocrystals: Soft Chemical Synthesis, Luminescent Properties, and Biomedical Applications. Chem Rev. 2014; 114: 2343–89.
47. Kömpe K, Borchert H, Storz J, et al. Green-Emitting CePO4:Tb/LaPO4 Core–Shell Nanoparticles with 70 % Photoluminescence Quantum Yield. Angew Chem Int Ed. 2003; 42: 5513–6.
48. Sun W, Yu J, Deng R, et al. Semiconducting Polymer Dots Doped with Europium Complexes Showing Ultranarrow Emission and Long Luminescence Lifetime for Time-Gated Cellular Imaging. Angew Chem Int Ed. 2013; 52: 11294–7.
49. Bonnet CS, Buron F, Caillé F, et al. Pyridine-Based Lanthanide Complexes Combining MRI and NIR Luminescence Activities. Chem A Eur J. 2012; 18: 1419–31.
50. Choi HS, Ipe BI, Misra P, Lee JH, Bawendi MG, Frangioni J V. Tissue- and Organ-Selective Biodistribution of NIR Fluorescent Quantum Dots. Nano Lett. 2009; 9: 2354–9.
51. Ruiz D, del Rosal B, Acebrón M, et al. Ag/Ag2S Nanocrystals for High Sensitivity Near-Infrared Luminescence Nanothermometry. Adv Funct Mater. 2017; 27: 1604629-9.
52. Shou K, Tang Y, Chen H, et al. Diketopyrrolopyrrole-based semiconducting polymer nanoparticles for *in vivo* second near-infrared window imaging and image-guided tumor surgery. Chem Sci. 2018; 9: 3105–10.
53. Luo S, Zhang E, Su Y, Cheng T, Shi C. A review of NIR dyes in cancer targeting and imaging. Biomaterials. 2011; 32: 7127–38.
54. Kanduluru AK, Srinivasarao M, Low PS. Design, Synthesis, and Evaluation of a Neurokinin-1 Receptor-Targeted Near-IR Dye for Fluorescence-Guided Surgery of Neuroendocrine Cancers. Bioconjug Chem. 2016; 27: 2157–65.
55. Sun L-D, Wang Y-F, Yan C-H. Paradigms and Challenges for Bioapplication of Rare Earth Upconversion Luminescent Nanoparticles: Small Size and Tunable Emission/Excitation Spectra. Acc Chem Res. 2014; 47: 1001–9.

56. Chen H-Q, Fu J, Wang L, et al. Ultrasensitive mercury(II) ion detection by europium(III)-doped cadmium sulfide composite nanoparticles. Talanta. 2010; 83: 139–44.
57. Wolska E, Kaszewski J, Kiełbik P, Grzyb J, Godlewski MM, Godlewski M. Rare earth activated ZnO nanoparticles as biomarkers. Opt Mater. 2014; 36: 1655–9.
58. Wang Y, Qin W, Zhang J, et al. Synthesis, photoluminescence and bioconjugation of rare-earth (Eu) complexes-embedded silica nanoparticles. Solid State Commun. 2007; 142: 689–93.
59. Rafique R, Kailasa SK, Park TJ. Recent advances of upconversion nanoparticles in theranostics and bioimaging applications. TrAC Trends Anal Chem. 2019; 120: 115646-19.
60. Skripka A, Karabanovas V, Jarockyte G, et al. Decoupling Theranostics with Rare Earth Doped Nanoparticles. Adv Funct Mater. 2019; 29: 1807105-12.
61. Zhao X, He S, Tan MC. Design of infrared-emitting rare earth doped nanoparticles and nanostructured composites. J Mater Chem C. 2016; 4: 8349–72.
62. Hemmer E, Venkatachalam N, Hyodo H, et al. Upconverting and NIR emitting rare earth based nanostructures for NIR-bioimaging. Nanoscale. 2013; 5: 11339–61.
63. Naczynski DJ, Tan MC, Riman RE, Moghe P V. Rare earth nanoprobes for functional biomolecular imaging and theranostics. J Mater Chem B. 2014; 2: 2958–73.
64. Chan MH, Liu RS. Advanced sensing, imaging, and therapy nanoplatforms based on Nd3+-doped nanoparticle composites exhibiting upconversion induced by 808 nm near-infrared light. Nanoscale. 2017; 9: 18153–68.
65. Wang Y, Wang H, Liu D, Song S, Wang X, Zhang H. Graphene oxide covalently grafted upconversion nanoparticles for combined NIR mediated imaging and photothermal/photodynamic cancer therapy. Biomaterials. 2013; 34: 7715–24.
66. Li X, Jiang M, Zeng S, Liu H. Polydopamine coated multifunctional lanthanide theranostic agent for vascular malformation and tumor vessel imaging beyond 1500 nm and imaging-guided photothermal therapy. Theranostics. 2019; 9: 3866–78.
67. Yin M, Ju E, Chen Z, Li Z, Ren J, Qu X. Upconverting Nanoparticles with a Mesoporous TiO2 Shell for Near-Infrared-Triggered Drug Delivery and Synergistic Targeted Cancer Therapy. Chem A Eur J. 2014; 20: 14012–7.
68. Mangeolle T, Yakavets I, Marchal S, et al. Fluorescent Nanoparticles for the Guided Surgery of Ovarian Peritoneal Carcinomatosis. Nanomaterials. 2018; 8: 572-20.
69. Zhou J, Shirahata N, Sun HT, et al. Efficient dual-modal NIR-to-NIR emission of rare earth ions co-doped nanocrystals for biological fluorescence imaging. J Phys Chem Lett. 2013; 4: 402–8.
70. Wang F, Liu X. Upconversion multicolor fine-tuning: Visible to near-infrared emission from lanthanide-doped NaYF4 nanoparticles. J Am Chem Soc. 2008; 130: 5642–3.
71. Takeshita S, Takebayashi Y, Nakamura H, Yoda S. Gas-Responsive Photoluminescence of YVO4:Eu3+ Nanoparticles Dispersed in an Ultralight, Three-Dimensional Nanofiber Network. Chem Mater. 2016; 28: 8466–9.
72. Ren G, Zeng S, Hao J. Tunable Multicolor Upconversion Emissions and Paramagnetic Property of Monodispersed Bifunctional Lanthanide-Doped NaGdF4 Nanorods. J Phys Chem C. 2011; 115: 20141–7.
73. Mi C-C, Tian Z, Han B, Mao C, Xu S. Microwave-assisted one-pot synthesis of water-soluble rare-earth doped fluoride luminescent nanoparticles with tunable colors. J Alloys Compd. 2012; 525: 154–8.
74. Liu S-M, Liu F-Q, Wang Z-G. Relaxation of carriers in terbium-doped ZnO nanoparticles. Chem Phys Lett. 2001; 343: 489–92.
75. Wang Y-F, Sun L-D, Xiao J-W, et al. Rare-Earth Nanoparticles with Enhanced Upconversion Emission and Suppressed Rare-Earth-Ion Leakage. Chem A Eur J. 2012; 18: 5558–64.
76. Qiu Z, Zhou Y, Lü M, Zhang A, Ma Q. Combustion synthesis of long-persistent luminescent MAl2O4: Eu2+, R3+ (M=Sr, Ba, Ca, R=Dy, Nd and La) nanoparticles and luminescence mechanism research. Acta Mater. 2007; 55: 2615–20.
77. Lécuyer T, Teston E, Ramirez-Garcia G, et al. Chemically engineered persistent luminescence nanoprobes for bioimaging. Theranostics. 2016; 6: 2488–524.
78. Buono-core GE, Li H, Marciniak B. Quenching of excited states by lanthanide ions and chelates in solution. Coord Chem Rev. 1990; 99: 55–87.
79. Yi G, Peng Y, Gao Z. Strong red-emitting near-infrared-to-visible upconversion fluorescent nanoparticles. Chem Mater. 2011; 23: 2729–34.
80. Abdukayum A, Chen J-T, Zhao Q, Yan X-P. Functional Near Infrared-Emitting Cr3+/Pr3+ Co-Doped Zinc Gallogermanate Persistent Luminescent Nanoparticles with Superlong Afterglow for *in Vivo* Targeted Bioimaging. J Am Chem Soc. 2013; 135: 14125–33.
81. Ni X, Zhang X, Duan X, Zheng HL, Xue XS, Ding D. Near-Infrared Afterglow Luminescent Aggregation-Induced Emission Dots with Ultrahigh Tumor-to-Liver Signal Ratio for Promoted Image-Guided Cancer Surgery. Nano Lett. 2019; 19: 318–30.
82. le Masne de Chermont Q, Chaneac C, Seguin J, et al. Nanoprobes with near-infrared persistent luminescence for *in vivo* imaging. Proc Natl Acad Sci. 2007; 104: 9266–71.
83. Lyu L, Cheong H, Ai X, et al. Near-infrared light-mediated rare-earth nanocrystals: recent advances in improving photon conversion and alleviating the thermal effect. NPG Asia Mater. 2018; 10: 685–702.
84. Shang X, Chen P, Jia T, et al. Upconversion luminescence mechanisms of Er3+ ions under excitation of an 800 nm laser. Phys Chem Chem Phys. 2015; 17: 11481–9.
85. Skripka A, Benayas A, Marin R, Canton P, Hemmer E, Vetrone F. Double rare-earth nanothermometer in aqueous media: opening the third optical transparency window to temperature sensing. Nanoscale. 2017; 9: 3079–85.
86. Kar A, Patra A. Impacts of core–shell structures on properties of lanthanide-based nanocrystals: crystal phase, lattice strain, downconversion, upconversion and energy transfer. Nanoscale. 2012; 4: 3608–19.
87. Ma D, Xu X, Hu M, et al. Rare-Earth-Based Nanoparticles with Simultaneously Enhanced Near-Infrared (NIR)-Visible (Vis) and NIR-NIR Dual-Conversion Luminescence for Multimodal Imaging. Chem An Asian J. 2016; 11: 1050–8.
88. Liu Z, Li B, Wang B, et al. Magnetic nanoparticles modified with DTPA-AMC-rare earth for fluorescent and magnetic resonance dual mode imaging. Dalt Trans. 2012; 41: 8723–8.
89. Kodaira CA, Loureno AVS, Felinto MCFC, et al. Biolabeling with nanoparticles based on Y2O3: Nd 3+ and luminescence detection in the near-infrared. J Lumin. 2011; 131: 727–31.
90. Soga K, Tokuzen K, Tsuji K, Yamano T, Hyodo H, Kishimoto H. NIR Bioimaging: Development of Liposome-Encapsulated, Rare-Earth-Doped Y2O3 Nanoparticles as Fluorescent Probes. Eur J Inorg Chem. 2010; 2010: 2673–7.
91. Dorman JA, Choi JH, Kuzmanich G, Chang JP. Elucidating the effects of a rare-earth oxide shell on the luminescence dynamics of Er3+ :Y2O3 nanoparticles. J Phys Chem C. 2012; 116: 10333–40.
92. Min Y-L, Wan Y, Yu S-H. Au@Y2O3:Eu3+ rare earth oxide hollow sub-microspheres with encapsulated gold nanoparticles and their optical properties. Solid State Sci. 2009; 11: 96–101.
93. Vetrone F, Boyer J-C, Capobianco JA, Speghini A, Bettinelli M. Concentration-Dependent Near-Infrared to Visible Upconversion in Nanocrystalline and Bulk Y2O3:Er3+. Chem Mater. 2003; 15: 2737–43.
94. Kumar GA, Chen CW, Ballato J, Riman RE. Optical characterization of infrared emitting rare-earth-doped fluoride nanocrystals and their transparent nanocomposites. Chem Mater. 2007; 19: 1523–8.
95. Wong H-T, Chan HLW, Hao J. Towards pure near-infrared to near-infrared upconversion of multifunctional GdF3:Yb3+,Tm3+ nanoparticles. Opt Express. 2010; 18: 6123–30.
96. Nyk M, Kumar R, Ohulchanskyy TY, Bergey EJ, Prasad PN. Photoluminescence Bioimaging Using Near Infrared to Near Infrared Up-Conversion in Tm3+ and Yb3+ Doped Fluoride Nanophosphors. Assay Drug Dev Technol. 2008; 3–6.
97. Zhan Q, He S, Qian J, Cheng H, Cai F. Optimization of optical excitation of upconversion nanoparticles for rapid microscopy and deeper tissue imaging with higher quantum yield. Theranostics. 2013; 3: 306—316.
98. Leary J, Key J. Nanoparticles for multimodal *in vivo* imaging in nanomedicine. Int J Nanomedicine. 2014; 9: 711-725.
99. Abdukayum A, Yang C-X, Zhao Q, Chen J-T, Dong L-X, Yan X-P. Gadolinium Complexes Functionalized Persistent Luminescent Nanoparticles as a Multimodal Probe for Near-Infrared Luminescence and Magnetic Resonance Imaging *in Vivo*. Anal Chem. 2014; 86: 4096–101.
100. Fan W, Yung B, Huang P, Chen X. Nanotechnology for Multimodal Synergistic Cancer Therapy. Chem Rev. 2017; 117: 13566–638.
101. Zhong Y, Ma Z, Zhu S, et al. Boosting the down-shifting luminescence of rare-earth nanocrystals for biological imaging beyond 1500 nm. Nat Commun. 2017; 8: 737-7.
102. Abdukayum A, Yang CX, Zhao Q, Chen JT, Dong LX, Yan XP. Gadolinium complexes functionalized persistent luminescent nanoparticles as a multimodal probe for near-infrared luminescence and magnetic resonance imaging *in vivo*. Anal Chem. 2014; 86: 4096–101.
103. Bunton J, Calvez L, Kadan V, Blonskyi I, Shpotyuk O, Golovchak R. Near-IR emission of Er3+ ions in CsCl-Ga-Ge-S glasses excited by visible light. Opt Mater. 2017; 72: 195–200.

104. Zhang M, Zheng W, Liu Y, et al. A New Class of Blue-LED-Excitable NIR-II Luminescent Nanoprobes Based on Lanthanide-Doped CaS Nanoparticles. Angew Chem Int Ed. 2019; 58: 9556–60.
105. Liu Y, Jia Q, Zhou J. Recent Advance in Near-Infrared (NIR) Imaging Probes for Cancer Theranostics. Adv Ther. 2018; 1: 1800055-21.
106. Liu L, Wang S, Zhao B, et al. Er3+ Sensitized 1530 nm to 1180 nm Second Near-Infrared Window Upconversion Nanocrystals for *In Vivo* Biosensing. Angew Chem Int Ed. 2018; 57: 7518–22.
107. Liu Y, Gong CS, Dai Y, et al. *In situ* polymerization on nanoscale metal-organic frameworks for enhanced physiological stability and stimulus-responsive intracellular drug delivery. Biomaterials. 2019; 218: 62-9.
108. Wenk CHF, Ponce F, Guillermet S, et al. Near-infrared optical guided surgery of highly infiltrative fibrosarcomas in cats using an anti-αvß3 integrin molecular probe. Cancer Lett. 2013; 334: 188–95.
109. Miao Q, Xie C, Zhen X, et al. Molecular afterglow imaging with bright, biodegradable polymer nanoparticles. Nat Biotechnol. 2017; 35: 1102–10.
110. Dang X, Gu L, Qi J, et al. Layer-by-layer assembled fluorescent probes in the second near-infrared window for systemic delivery and detection of ovarian cancer. Proc Natl Acad Sci. 2016; 113: 5179–84.
111. Naczynski DJ, Tan MC, Zevon M, et al. Rare-earth-doped biological composites as *in vivo* shortwave infrared reporters. Nat Commun. 2013; 4: 2199-10.
112. Yang L, Wang J, Yang S, Lu Q, Li P, Li N. Rod-shape MSN@MoS2 Nanoplatform for FL/MSOT/CT Imaging-Guided Photothermal and Photodynamic Therapy. Theranostics. 2019; 9: 3992-4005.
113. Chen Q, Liang C, Wang X, He J, Li Y, Liu Z. An albumin-based theranostic nano-agent for dual-modal imaging guided photothermal therapy to inhibit lymphatic metastasis of cancer post surgery. Biomaterials. 2014; 35: 9355–62.
114. Thimsen E, Sadtler B, Berezin MY. Shortwave-infrared (SWIR) emitters for biological imaging: a review of challenges and opportunities. Nanophotonics. 2017; 6: 1043–54.
115. Zhao M, Li B, Wang P, et al. Supramolecularly Engineered NIR-II and Upconversion Nanoparticles *In Vivo* Assembly and Disassembly to Improve Bioimaging. Adv Mater. 2018; 30: 1804982-8.
116. Zhao M, Wang R, Li B, et al. Precise *In Vivo* Inflammation Imaging Using *In Situ* Responsive Cross-linking of Glutathione-Modified Ultra-Small NIR-II Lanthanide Nanoparticles. Angew Chem. 2019; 131: 2072–6.
117. Li Y, Zeng S, Hao J. Non-Invasive Optical Guided Tumor Metastasis/Vessel Imaging by Using Lanthanide Nanoprobe with Enhanced Down-Shifting Emission beyond 1500 nm. ACS Nano. 2019; 13: 248–59.
118. Gu Y, Guo Z, Yuan W, et al. High-sensitivity imaging of time-domain near-infrared light transducer. Nat Photonics. 2019; 13: 525–31.
119. Chao J, Zhu D, Zhang Y, Wang L, Fan C. DNA nanotechnology-enabled biosensors. Biosens Bioelectron. 2016; 76: 68–79.
120. Yuan Q, Wu Y, Wang J, et al. Targeted Bioimaging and Photodynamic Therapy Nanoplatform Using an Aptamer-Guided G-Quadruplex DNA Carrier and Near-Infrared Light. Angew Chem Int Ed. 2013; 52: 13965–9.
121. Tang Y, Hu H, Zhang MG, et al. An aptamer-targeting photoresponsive drug delivery system using "off–on" graphene oxide wrapped mesoporous silica nanoparticles. Nanoscale. 2015; 7: 6304–10.
122. Yang Y, Liu G, Liu H, Li D, Fan C, Liu D. An Electrochemically Actuated Reversible DNA Switch. Nano Lett. 2010; 10: 1393–7.
123. Liu Q, Ge Z, Mao X, et al. Valency-Controlled Framework Nucleic Acid Signal Amplifiers. Angew Chem Int Ed. 2018; 57: 7131–5.
124. Liang L, Li J, Li Q, et al. Single-Particle Tracking and Modulation of Cell Entry Pathways of a Tetrahedral DNA Nanostructure in Live Cells. Angew Chem Int Ed. 2014; 53: 7745–50.
125. Qu X, Yang F, Chen H, et al. Bubble-Mediated Ultrasensitive Multiplex Detection of Metal Ions in Three-Dimensional DNA Nanostructure-Encoded Microchannels. ACS Appl Mater Interfaces. 2017; 9: 16026–34.
126. Fu Y, Zeng D, Chao J, et al. Single-Step Rapid Assembly of DNA Origami Nanostructures for Addressable Nanoscale Bioreactors. J Am Chem Soc. 2013; 135: 696–702.
127. Qu A, Sun M, Xu L, et al. Quantitative zeptomolar imaging of miRNA cancer markers with nanoparticle assemblies. Proc Natl Acad Sci. 2019; 116: 3391-400.
128. He L, Brasino M, Mao C, et al. DNA-Assembled Core-Satellite Upconverting-Metal–Organic Framework Nanoparticle Superstructures for Efficient Photodynamic Therapy. Small. 2017; 13: 1700504-7.
129. He L, Dragavon J, Cho S, et al. Self-assembled gold nanostar–NaYF4:Yb/Er clusters for multimodal imaging, photothermal and photodynamic therapy. J Mater Chem B. 2016; 4: 4455–61.
130. Chen N, Wei M, Sun Y, et al. Self-Assembly of Poly-Adenine-Tailed CpG Oligonucleotide-Gold Nanoparticle Nanoconjugates with Immunostimulatory Activity. Small. 2014; 10: 368–75.
131. Huang Y, Li M, Huang D, et al. Depth-Resolved Enhanced Spectral-Domain OCT Imaging of Live Mammalian Embryos Using Gold Nanoparticles as Contrast Agent. Small. 2019; 15: 1902346-13.
132. Rinker S, Ke Y, Liu Y, Chhabra R, Yan H. Self-assembled DNA nanostructures for distance-dependent multivalent ligand–protein binding. Nat Nanotechnol. 2008; 3: 418–22.
133. Wilner OI, Willner I. Functionalized DNA Nanostructures. Chem Rev. 2012; 112: 2528–56.
134. Edwardson TGW, Lau KL, Bousmail D, Serpell CJ, Sleiman HF. Transfer of molecular recognition information from DNA nanostructures to gold nanoparticles. Nat Chem. 2016; 8: 162.
135. Langecker M, Arnaut V, Martin TG, et al. Synthetic Lipid Membrane Channels Formed by Designed DNA Nanostructures. Science. 2012; 338: 932–6.
136. Goodman RP, Heilemann M, Doose S, Erben CM, Kapanidis AN, Turberfield AJ. Reconfigurable, braced, three-dimensional DNA nanostructures. Nat Nanotechnol. 2008; 3: 93–6.
137. Ye D, Li L, Li Z, et al. Molecular Threading-Dependent Mass Transport in Paper Origami for Single-Step Electrochemical DNA Sensors. Nano Lett. 2019; 19: 369–74.
138. Li L-L, Wu P, Hwang K, Lu Y. An Exceptionally Simple Strategy for DNA-Functionalized Up-Conversion Nanoparticles as Biocompatible Agents for Nanoassembly, DNA Delivery, and Imaging. J Am Chem Soc. 2013; 135: 2411–4.
139. Sun M, Hao T, Li X, et al. Direct observation of selective autophagy induction in cells and tissues by self-assembled chiral nanodevice. Nat Commun. 2018; 9: 4494-10.
140. McDannold N, Zhang Y, Supko JG, et al. Acoustic feedback enables safe and reliable carboplatin delivery across the blood-brain barrier with a clinical focused ultrasound system and improves survival in a rat glioma model. Theranostics. 2019; 9: 6284-99.
141. Yang Z, Fan W, Zou J, et al. Precision Cancer Theranostic Platform by *In Situ* Polymerization in Perylene Diimide-Hybridized Hollow Mesoporous Organosilica Nanoparticles. J Am Chem Soc. 2019; 141: 14687–98.
142. Sun W, Luo L, Feng Y, et al. Aggregation-Induced Emission Gold Clustoluminogens for Enhanced Low-Dose X-ray-Induced Photodynamic Therapy. Angew Chem Int Ed. 2019; in press. doi:10.1002/anie.201908712
143. Azad MB, Chen Y, Gibson SB. Regulation of Autophagy by Reactive Oxygen Species (ROS): Implications for Cancer Progression and Treatment. Antioxid Redox Signal. 2008; 11: 777–90.
144. Wang C, Cheng L, Liu Z. Upconversion nanoparticles for photodynamic therapy and other cancer therapeutics. Theranostics. 2013; 3: 317–30.
145. Liu J, Bu W, Pan L, Shi J. NIR-Triggered Anticancer Drug Delivery by Upconverting Nanoparticles with Integrated Azobenzene-Modified Mesoporous Silica. Angew Chem Int Ed. 2013; 52: 4375–9.
146. Yan B, Boyer J-C, Branda NR, Zhao Y. Near-Infrared Light-Triggered Dissociation of Block Copolymer Micelles Using Upconverting Nanoparticles. J Am Chem Soc. 2011; 133: 19714–7.
147. Yu Z, Ge Y, Sun Q, et al. A pre-protective strategy for precise tumor targeting and efficient photodynamic therapy with a switchable DNA/upconversion nanocomposite. Chem Sci. 2018; 9: 3563–9.
148. Staninec M, Douglas SM, Darling CL, et al. Non-destructive clinical assessment of occlusal caries lesions using near-IR imaging methods. Lasers Surg Med. 2011; 43: 951–9.
149. Ma M, Gao N, Sun Y, Ren J, Qu X. A Near-Infrared Responsive Drug Sequential Release System for Better Eradicating Amyloid Aggregates. Small. 2017; 13: 1701817.
150. Wang P, Fan Y, Lu L, et al. NIR-II nanoprobes in-vivo assembly to improve image-guided surgery for metastatic ovarian cancer. Nat Commun. 2018; 9: 2898-10.
151. Li D, He S, Wu Y, et al. Excretable Lanthanide Nanoparticle for Biomedical Imaging and Surgical Navigation in the Second Near-Infrared Window. Adv Sci. 2019; 0: 1902042. in press. doi:10.1002/advs.201902042.
152. Wang P, Wang X, Luo Q, et al. Fabrication of Red Blood Cell-Based Multimodal Theranostic Probes for Second Near-Infrared Window Fluorescence Imaging-Guided Tumor Surgery and Photodynamic Therapy. Theranostics. 2019; 9: 369-380.
153. Gargas DJ, Chan EM, Ostrowski AD, et al. Engineering bright sub-10-nm upconverting nanocrystals for single-molecule imaging. Nat Nanotechnol. 2014; 9: 300-5.
154. Feng Y, Chen F, Ma Z, et al. Towards stratifying ischemic components by cardiac MRI and multifunctional stainings in a rabbit model of myocardial infarction. Theranostics. 2013; 4: 24-35.
155. Dewitte H, Vanderperren K, Haers H, et al. Theranostic mRNA-loaded microbubbles in the lymphatics of dogs: implications for drug delivery. Theranostics. 2015; 5: 97-109.

156. Hong G, Robinson JT, Zhang Y, et al. *In vivo* fluorescence imaging with Ag2S quantum dots in the second near-infrared region. Angew Chem Int Ed. 2012; 51: 9818–21.